9-1-2021

Simulation of anisoplanatic lucky look imaging and statistics through optical turbulence using numerical wave propagation

Michael A. Rucci
Air Force Research Laboratory

Russell C. Hardie
University of Dayton, rhardie1@udayton.edu

Richard K. Martin
United States Air Force Institute of Technology

Simulation of anisoplanatic lucky look imaging and statistics through optical turbulence using numerical wave propagation

MICHAEL A. RUCCI[1,3,*], RUSSELL C. HARDIE[2], AND RICHARD K. MARTIN[3]

[1] Air Force Research Laboratory, AFRL/RYMT, Building 620, 2241 Avionics Circle, Wright-Patterson AFB, Ohio 45433, USA
[2] University of Dayton, Department of Electrical and Computer Engineering, 300 College Park, Dayton, Ohio 45459, USA
[3] Air Force Institute of Technology, Department of Electrical Engineering, 2950 Hobson Way, Dayton, Ohio 45433, USA
[*] Corresponding author: michael.rucci@us.af.mil

Compiled November 12, 2021

This paper investigates anisoplanatic numerical wave simulation in the context of lucky look imaging. We demonstrate that numerical wave propagation can produce root mean square (RMS) wavefront distributions and probability of lucky look (PLL) statistics that are consistent with Kolmogorov theory. However, the simulated RMS statistics are sensitive to the sampling parameters used in the propagation window. To address this, we propose and validate a new sample spacing rule based on the point source bandwidth used in the propagation and the level of atmospheric turbulence. We use the tuned simulator to parameterize the wavefront RMS probability density function as a function of turbulence strength. The fully parameterized RMS distribution model is used to provide a way to accurately predict the PLL for a range of turbulence strengths. We also propose and validate a new parametric average lucky look optical transfer function (OTF) model that could be used to aid in image restoration. Our OTF model blends the theoretical diffraction-limited OTF and the average turbulence short exposure OTF. Finally, we show simulated images for several anisoplanatic imaging scenarios that reveal the spatially varying nature of the RMS values impacting local image quality.

http://dx.doi.org/10.1364/ao.XX.XXXXXX

1. INTRODUCTION

The simulation of atmospheric optical turbulence is vital in understanding the impact of turbulence on imaging systems and developing and evaluating turbulence mitigation algorithms. A powerful method for turbulence simulation uses numerical wave propagation [1]. Here, a point source model is numerically propagated through a series of phase screens to the camera pupil plane. The pupil plane phase ultimately forms a point spread function (PSF) that is used to simulate image degradation. Recently, this approach has been extended to anisoplanatic imaging scenarios for wide field-of-view terrestrial imaging applications [2, 3]. In the anisoplanatic case, an array of point sources in the object plane are propagated through extended phase screens to create spatially varying PSFs with accurate spatial correlation between PSFs. These methods have been validated using metrics such as isoplanatic angle, tilt variance, tilt correlation, and optical transfer function (OTF) analyses [3].

However, one important validation metric not previously considered is the distribution of the pupil-plane wavefront phase error. This distribution captures the variation in the level of degradation introduced by the simulated pupil plane wavefronts. Closely related to the distribution of the wavefront phase error is the probability of lucky look (PLL). A lucky look is defined by Fried [4] as a tilt-corrected pupil plane wavefont

phase root-mean-square (RMS) value less than or equal to 1 radian. We believe matching the theoretical wavefront phase error distribution and PLL are critically important for a simulator when studying turbulence and turbulence mitigation algorithms. We find this is possible, but only with careful choices of the wavefront sample spacing and the number of wavefont samples used for propagation. In this paper, we propose closed-form equations for these sampling parameters and demonstrate that they produce simulated wavefront phase RMS value distribution and PLL that closely match the distribution obtained with an independent Zernike analysis and with values reported by Fried [4]. The proposed sampling rules are based on the bandwidth of the point source used for propagation and the level of turbulence indicated by the Fried parameter, r_0.

In the study of lucky look imaging, we believe it is valuable to have a model for the probability density function (PDF) of the RMS wavefront phase for a given turbulence strength. A three-parameter gamma function has been shown to yield close fitting to RMS wavefront phase in the astronomy case where tip and tilt are removed with an adaptive optic [5]. The previous form of the three-parameter gamma function relied on calculating statics of empirically measured RMS distributions in order to fit the three parameters. Using our tuned numerical-wave simulator, we are able to generate large quantities of wavefront RMS data. This allows us to generate a densely sampled wavefront phase RMS distribution for a wide range of turbulence strengths. We use these data to generate closed form expressions for the three parameters of the gamma PDF as a function of turbulence strength. In turn, this enables us to calculate the PLL values for a continuous range of turbulence strengths. This helps to fill in the PLL values between those reported for discrete turbulence levels in Fried's original landmark work [4] for the weak turbulence regime. Our model also matches well with Fried's closed form PLL expression that applies only to higher turbulence levels.

Another important aspect of modeling lucky look imaging is an OTF analysis. Here we propose a parametric model for the average lucky look OTF. Our model blends the theoretical diffraction-limited OTF [6] and the average turbulence short exposure OTF [7]. We show that the blending parameter, β, can be expressed in terms of Strehl ratios and ultimately the wavefront RMS PDFs mentioned above. Using the simulator we validate the proposed lucky look OTF. We believe the parametric lucky look OTF model can be used to better understand lucky look imaging and to aid in image restoration for turbulence mitigation.

The rest of the paper is organized as follows. Section 2 discusses the calculation of the pupil plane wavefont statistics and modeling the average lucky look OTF. The numerical wave propagation sampling parameters are introduced in Section 3. Section 4 shows the experimental results that include the wavefront RMS fitting and PLL analysis. Also presented is an empirical validation of the lucky look OTF model. Section 4 concludes with anisoplanatic image simulation results that reveal the spatially varying nature of the RMS values impacting local image quality. Finally, we offer overall conclusions in Section 5.

2. LUCKY LOOK STATISTICS

In this section we present the relevant lucky look statistics. We begin with a Zernike wavefront phase model since we use this to help validate the numerical wave simulator and the resulting RMS distributions.

A. Zernike Wavefront Phase Model

A commonly used approach to modeling the wavefront phase for a variety of applications, including imaging in turbulence, is to express the wavefront phase as a weighted sum of 2D Zernike polynomials. One can use this approach to not only model the wavefront phases, but to also simulate realizations of wavefront phases for statistical analyses. We follow the approach presented by Roddier [8], who built upon the earlier work of Noll [9].

One can use a finite number, J, of Zernike polynomials to produce wavefronts that seek to capture the Kolmogorov spectrum of atmospheric turbulence. Roddier [8] shows that a $J \times J$ covariance matrix, $\mathbf{C}$, is required to generate the appropriate weightings of the Zernike polynomials. The covariance is dependent on the system aperture, D, and coherence diameter of the atmosphere, r_0, also referred to as Fried's parameter. We refer the reader to [8] for the exact form of the covariance matrix. Roddier uses a singular value decomposition (SVD) to produce $\mathbf{C} = \mathbf{USV}^T$, where $\mathbf{U}$ and $\mathbf{V}$ are unitary. The matrix $\mathbf{S}$ is a diagonal matrix containing eigenvalue terms of the Karhunen-Loéve function, and $\mathbf{s} = \text{diag}(\mathbf{S})$.

Now consider a $J \times 1$ Gaussian random vector, $\mathbf{b}$, with independent identically distributed (i.i.d.) elements. Let the variances of the elements in $\mathbf{b}$ be given by the corresponding elements in $\mathbf{s}$ from the SVD analysis mentioned above. A vector of Zernike polynomial weightings can then be defined as

$$\mathbf{n} = \mathbf{U}^T\mathbf{b}, \tag{1}$$

where $\mathbf{n} = [n_1, n_2, ...n_J]^T$. A single random atmospheric wavefront phase, $\boldsymbol{\phi}(x, y)$, can be calculated using the weights in Eq. (1) as

$$\boldsymbol{\phi}(x, y) = \sum_{j=4}^{J} n_j Z_j(x, y), \tag{2}$$

where x, y are the continuous spatial coordinates in the pupil plane. The term $Z_j(x, y)$ represents the $j'th$ Zernike function. Note that our summation excludes $j = 1$ to omit the contribution of the piston term, $Z_1(x, y)$, as we are interested in the incoherent imaging scenario. Additionally, the Zernike tip/tilt terms, defined as $Z_2(x, y)$ and $Z_3(x, y)$, are also removed in Eq. (2) as they solely lead to PSF displacement, not blur.

The RMS metric is commonly used to quantify the wavefront distortion that controls the amount of blur from optical aberrations. The RMS of $\boldsymbol{\phi}(x, y)$ may be expressed as

$$\Delta_\phi = \left(\frac{4}{\pi D^2}\iint_A (\boldsymbol{\phi}(x, y))^2 dxdy\right)^{1/2}, \tag{3}$$

where A is such that $(x, y) \in A$ spans the aperture area. Fried's [4] definition for the isoplanatic PLL can then be calculated as

$$\text{Prob(good short-exposure image)} = \text{Prob}\left(\Delta_\phi \leq 1 \text{ rad}\right) \tag{4}$$

for a single turbulent wavefront phase. Fried used a Monte Carlo analysis to compute PLLs, as reported in [4]. Some of Fried's computed PLLs are also listed here in Sect. 4. In the original work, Fried generated wavefront phases using an approach similar to the Zernike model in Eq. (2). However, instead of Zernike polynomials, a specially designed set of othonormal polynomials was computed and used. It has been shown that the Zernike representation closely matches the orthonormal polynomials originally used by Fried [10].

As one might expect, the PLL drops as the turbulence strength increases. Fried fit a curve to the data in his Monte Carlo analysis and offers a convenient closed-form expression for the PLL for moderate to higher turbulence levels. In particular, Fried states that for $D/r_0 \geq 3.5$ the PLL can be approximated by

$$\text{Prob}\left(\Delta_\phi \leq 1 \text{ rad}\right) \approx 5.6 \exp[-0.1557(D/r_0)^2]. \tag{5}$$

As we will show in Sec. 4, this expression is accurate for high turbulence levels, but is not representative in the weaker turbulence regime that is common in terrestrial imaging applications.

B. RMS and Strehl Ratio

The probability of a lucky look could also be calculated from a PDF, $f_{\Delta_\phi}(r)$, that represents the density of the RMS values, r, calculated from the tip/tilt removed phase contributions in the pupil plane for a given D/r_0 where

$$\text{Prob}(\Delta_\phi \leq 1 \text{ rad}) = \int_0^1 f_{\Delta_\phi}(\xi) d\xi. \tag{6}$$

Astronomical imaging of a star with a Shack-Hartman sensor and adaptive optic [5] produced RMS phase distributions for a set D/r_0. The RMS phase distributions in [5] and [11] have a heavy tail towards higher RMS values. Gladysz, et al., [5] demonstrated a gamma function can closely match the RMS PDF, $f_{\Delta_\phi}(r)$, using three parameters; k defining the shape parameter, θ being the scale parameter, and μ shifting the PDF. The three-parameter gamma discussed in [5] is given as

$$f_{\Delta_\phi}(r; k, \theta, \mu) = \frac{\left(\frac{r-\mu}{\theta}\right)^{k-1} \exp\left(-\frac{r-\mu}{\theta}\right)}{\Gamma(k)\theta} \tag{7}$$

for $r \geq \mu$ with the gamma function, $\Gamma(k)$, calculated as

$$\Gamma(k) = \int_0^\infty t^{k-1} e^{-t} dt. \tag{8}$$

Two useful calculations, utilized later in this section, are the expected value of the three parameter gamma PDF,

$$\mathrm{E}[\Delta_\phi] = \int_0^\infty r f_{\Delta_\phi}(r) dr, \tag{9}$$

and the average lucky RMS value for a threshold, b,

$$\mathrm{E}[\Delta_\phi | \Delta_\phi \leq b] = \frac{\int_0^b r f_{\Delta_\phi}(r) dr}{\int_0^b f_{\Delta_\phi}(r) dr}. \tag{10}$$

Note that we use a threshold of b here, rather than 1, as a generalization of Fried's original lucky look definition.

A third option in determining the PLL is accomplished by examining the Strehl ratio [12]. The Strehl ratio is generally used in astronomy where a very small star acts as point source to produce a turbulent point spread function (PSF) seen in the image plane. Imaging a point source when no turbulence is present results in seeing a diffraction limited PSF. The diffraction limited case reveals the best resolution possible through the camera and generally has a tight core whereas the turbulent PSF has a more scattered core [13]. A single random atmospheric wavefront phase calculated in Eq. (2) can be transformed into a turbulent PSF, $h_\phi(x, y)$, following the process described in [14]. The Strehl ratio can be calculated for a single turbulent PSF as

$$s_\phi = \frac{\max_{(x,y)}[h_\phi(x, y)]}{\max_{(x,y)}[h_{dif}(x, y)]}, \tag{11}$$

where the use of the $h_{dif}(x, y)$ in the denominator bounds $0 \leq s_\phi \leq 1$ since diffraction limited is the best possible resolution. A useful conversion between the Strehl ratio and the corresponding wavefront phase RMS can be calculated as

$$s_\phi \approx \exp(-\Delta_\phi^2) \tag{12}$$

using the Maréchal approximation [15]. The average Strehl ratio can be calculated using Eq. (12) to transform $f_{\Delta_\phi}(r; k, \theta, \mu)$ to $f_{s_\phi}(q; k, \theta, \mu)$ [16] to give the formula

$$f_{s_\phi}(q; k, \theta, \mu) = f_{\Delta_\phi}(\sqrt{-\ln(q)}; k, \theta, \mu)(2q\sqrt{-\ln(q)})^{-1} \tag{13}$$

with the expected value

$$\mathrm{E}[s_\phi] = \int_0^1 q f_{s_\phi}(q; k, \theta, \mu) dq = \int_0^1 f_{\Delta_\phi}(\sqrt{-\ln(q)}; k, \theta, \mu)(2\sqrt{-\ln(q)})^{-1} dq. \tag{14}$$

The average lucky look Strehl ratio can be computed using the same approach as that in Eq. (10) but with the PDF from Eq. (13) and a transformed threshold of $p \approx \exp(-b^2)$ from Eq. (12). This gives rise to

$$\mathrm{E}[s_\phi | s_\phi \geq p] = \frac{\int_p^1 f_{\Delta_\phi}(\sqrt{-\ln(q)}; k, \theta, \mu)(2\sqrt{-\ln(q)})^{-1} dq}{\int_p^1 f_{\Delta_\phi}(\sqrt{-\ln(q)}; k, \theta, \mu)(2q\sqrt{-\ln(q)})^{-1} dq}. \tag{15}$$

C. Optical Transfer Function

Let us now turn our attention to an OTF analysis for lucky look imaging. First, the diffraction-limited OTF is defined in [6] as

$$H_{dif}(\rho) = \begin{cases} \frac{2}{\pi}\left[\cos^{-1}\left(\frac{\rho}{\rho_c}\right) - \frac{\rho}{\rho_c}\sqrt{1 - \left(\frac{\rho}{\rho_c}\right)^2}\right] & \rho \leq \rho_c \\ 0 & \text{else} \end{cases}, \tag{16}$$

with $\rho = \sqrt{u^2 + v^2}$ and u and v being continuous spatial frequencies in units of cycles per unit distance. The optical cutoff frequency is given by $\rho_c = 1/(\lambda f/\#)$ with the f-number $f/\#$ being calculated as the ratio of the focal length, l, over the aperture diameter, D. The average short exposure OTF [7] is

$$\langle H_{Turb}(\rho)\rangle_{SE,\alpha} = \exp\left\{-3.44\left(\frac{\lambda l \rho}{r_0}\right)^{5/3}\left[1-\alpha\left(\frac{\lambda l \rho}{D}\right)^{1/3}\right]\right\} \tag{17}$$

where α controls the characteristics of the average short exposure OTF. Fried[7] uses $\alpha = 1$ for a near-field approximation when $D \gg \sqrt{L\lambda}$. A value of $\alpha = 1/2$ is used for the far field approximation. In the context of multi-frame turbulence mitigation, α has been viewed as a tilt correction factor from registration[17]. There a value of $\alpha = 1$ would represent perfect tilt correction and a true near-field short exposure OTF. If no registration is used, but image fusion is still applied, one could set $\alpha = 0$ and this would be equivalent to a long exposure OTF[7].

We proposed a new average lucky look OTF model by blending Eqs. (16) and (17). This OTF model is given by

$$\langle H_{Turb}(u,v)\rangle_{LL,\alpha,\beta} = H_{dif}(u,v)(\beta + (1-\beta)\langle H_{Turb}(u,v)\rangle_{SE,\alpha}), \tag{18}$$

where $0 \leq \beta \leq 1$ is the blending parameter. A smaller β gives more weight to the average short exposure OTF, while a larger β gives more weight to the diffraction OTF. We believe this is an intuitive model that allows us to have a parametric model for lucky look imaging scenarios that can aid in image restoration for turbulence mitigation. Interestingly, the blending parameter, β, can be related to Strehl ratios and ultimately the RMS PDFs from Sec. 2.B. To show this, consider that the Strehl ratio from Eq. (11) can also be expressed in terms of the OTFs [12]. Taking the double integral of both sides of Eq. (18) and normalizing by the diffraction OTF we obtain

$$\frac{\int\int \langle H_{Turb}(u,v)\rangle_{LL,\alpha,\beta} dudv}{\int\int H_{dif}(u,v)dudv} = \frac{\int\int H_{dif}(u,v)(\beta + (1-\beta)\langle H_{Turb}(u,v)\rangle_{SE,\alpha})dudv}{\int\int H_{dif}(u,v)dudv}. \tag{19}$$

Then using the OTF-based Strehl ratio definition [12] we can express this in terms of the ensemble-average Strehl ratios as

$$\langle s_{LL}\rangle = 1\beta + (1-\beta)\langle s_{SE}\rangle. \tag{20}$$

This can be expressed alternatively as

$$\mathrm{E}[s_\phi | s_\phi \geq p] = 1\beta + (1-\beta)\mathrm{E}[s_\phi]. \tag{21}$$

Solving for β we obtain

$$\beta = \frac{\mathrm{E}[s_\phi | s_\phi \geq p] - \mathrm{E}[s_\phi]}{1 - \mathrm{E}[s_\phi]}. \tag{22}$$

Note that β in Eq. (22) can be calculated using the three parameter gamma PDF introduced in Sec. 2.B using Eqs. (14) and (15). In Sec. 4.B we provide the necessary calculations for k, θ, and μ for a given D/r_0. We also show in Sec. 4.B that there is close agreement between the model in Eq. (18) and the empirical lucky look OTF generated from simulated data. We believe the proposed model for $\langle H_{Turb}(u,v)\rangle_{LL,\alpha,\beta}$ in Eq. (18) is very intuitive and flexible. Using the parameter β we are able to adjust for the level of lucky look specificity that may be employed. Also, the parameter α gives control over the nature of the assumed average short exposure OTF. It should be noted that the model in Eq. (18) assumes a nominally diffraction-limited imaging system when no turbulence is present. This is consistent with the anisoplanatic simulator used in our validation study. However, for other applications, one can readily augment the model in Eq. (18) to incorporate other OTF components such as defocus, optical aberrations, or atmospheric aerosols [18]. These OTF components could be multiplied by the model in Eq. (18) to limit the upper bound on the overall OTF.

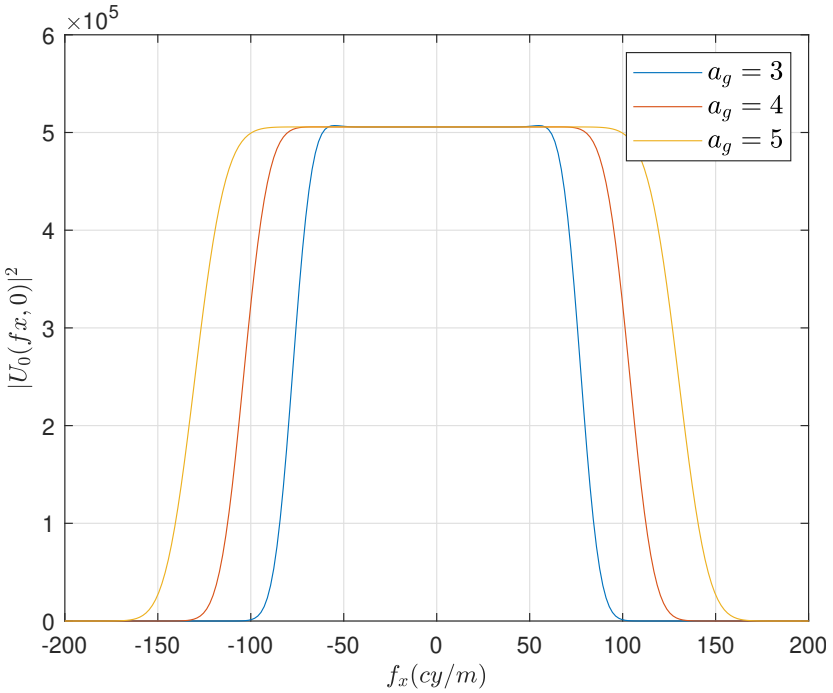

Fig. 1. Single axis slice through the magnitude of the point source in the frequency domain for three different a_g values.

3. NUMERICAL WAVE PROPAGATION SAMPLING

The wave propagation simulator employed here [3] utilizes a 2-D Gaussian windowed sinc function, $u_0(x,y)$, with quadratic phase as its point source [1]. This is calculated in the spatial domain as

$$u_0(x,y) = \left(\frac{D_1^2}{\lambda L}\right) e^{-\frac{jk}{2L}(x^2+y^2)} \text{sinc}\left(x\left(\frac{D_1}{\lambda L}\right)\right) \times \text{sinc}\left(y\left(\frac{D_1}{\lambda L}\right)\right) e^{-\frac{(D_1/\lambda L)^2}{16}(x^2+y^2)}, \tag{23}$$

where L is the propagation distance, λ is the wavelength of light, k is the wavenumber. The parameter D_1 is the width of the uniform wavefront span at the pupil plane that results from a propagation of the point source due exclusively to diffraction with no turbulence.

Schmidt [1] states that D_1 must be larger than the optical systems aperture, D, and is generally calculated using an aperture gain, a_g, as $D_1 = a_g D$ with $a_g > 1$. The 2-D Gaussian windowed sinc function spatial cutoff frequency, $f_{x,\text{max}}$, for a single axis is driven by D_1 such that

$$f_{x,\text{max}} = \frac{D_1}{2\lambda L} = \frac{a_g D}{2\lambda L}. \tag{24}$$

The Nyquist sampling spacing [19] for Eq. (23) in a vacuum propagation is then

$$\Delta x = \frac{1}{2f_{x,\text{max}}} = \frac{\lambda L}{a_g D}. \tag{25}$$

The impact of a_g on $U_0(f_x, f_y)$, the Fourier transform of $u_0(x,y)$, is plotted in Fig. 1 showing how a larger a_g will lead to a higher cutoff frequency.

Numerical wave propagation through atmospheric turbulence needs to include an additional term that captures the added angular spreading induced by turbulence [20]. Schmidt [1] references the work of [20]

where the apertures for a horizontal simulation grow by

$$D_1' = D_1 + c\frac{\lambda L}{r_0} \tag{26}$$

and

$$D' = D + c\frac{\lambda L}{r_0}, \tag{27}$$

where the scalar, c, indicates the overall simulation sensitivity to turbulence. The growth of the point source diameter in Eq. (26) modifies the Nyquist sampling in Eq. (25) to produce

$$\Delta x_{r_0} = \frac{\lambda L}{a_g D + c\frac{\lambda L}{r_0}}, \tag{28}$$

where the sampling rate decreases as the turbulence strength increases. Intuitively, this makes sense as stronger levels of turbulence require finer sampling of the turbulence phase screens in order to produce the correct turbulent PSFs.

The original spatial sampling rate used in [3] was derived in [19] as

$$\Delta x_v = \sqrt{\frac{\lambda L}{\mathscr{N}}}. \tag{29}$$

Although Eq. (28) removes the number of samples across the propagation window, $\mathscr{N}$, from the calculation of Δx_{r_0}, compared to Eq. (29), care must still be taken to ensure there are enough samples across the phase screens and aperture plane to allow for correct 2-D Fourier transforms. Schmidt [1] explains the number of samples in the simulation must follow the inequality, for a constant Δx_{r_0}, as

$$\mathscr{N}_{r_0} \geq \frac{D_1' + D'}{2\Delta x_{r_0}} + \frac{\lambda L}{2(\Delta x_{r_0})^2}, \tag{30}$$

where a larger D/r_0 will require a larger $\mathscr{N}_{r_0}$ and smaller Δx_{r_0} to properly sample the simulation, as shown in Sect. 4.

A final consideration in setting Δx_{r_0} for a simulation is whether the Kolmogorov or von Karman model is used to generate the phase screens. Kolmogorov turbulence dictates the inner scale of the PSD model to be zero, while von Karman allows for a non-zero inner scale value. Knepp [21] suggests the Δx_{r_0} parameter must be smaller than the inner scale, l_0, value using the inequality $\Delta x_{r_0} < l_0/3$ to adequately model the turbulent phase.

4. EXPERIMENTAL RESULTS

Optical parameters and the majority of simulation parameters used in this paper are the same as in [3]. The optical simulation parameters are listed in Table 1 while any variations to the simulation parameters are listed in Table 2. The numerical wave propagation turbulence simulator [3] was upgraded to properly calculate pupil plane wavefront phase RMS. A two-dimensional phase unwrapping algorithm [22] was used to unwrap the pupil plane phase. The unwrapped phase was then detrended using a least squares 2D plane fitting approach to remove the tip/tilt component.

A. Simulating Lucky Look Anisoplanatic Turbulence

The numerical wave propagation simulator generated 10,000 independent turbulent wavefront phase realizations, and corresponding PSFs, for a given D/r_0, a_g, and range of Δx's. Results from these trials produced a single optimal $\Delta\hat{x}$ generating the correct PLL. The large number of independent realizations was required to ensure an accurate PLL calculation and a highly populated histogram. Table 2 shows how the new Δx_{r_0} calculated from Eq. (28) is closer to the optimal $\Delta\hat{x}$ value than Δx_v used in [3]. This is due to the fact that

Table 1. Optical parameters.

Parameter	Value
Aperture	$D = 0.2034$ m
Focal length	$l = 1.2$ m
F-number	$f/\# = 5.9$
Wavelength	$\lambda = 0.525$ μm
Object distance	$L = 7$ km
Nyquist pixel spacing (focal plane)	$\delta_f = 1.5488$ μm
Nyquist pixel spacing (object plane)	$\delta_f = 9.0344$ μm

Voelz [19] utilized a chirp function as the point source versus a Gaussian windowed sinc function and did not include the impact of turbulence. It is interesting to note the PLL's sensitivity with the choice of Δx_{r_0} shown in Table 2. Relatively small changes in the Δx_{r_0} parameter can lead to the incorrect PLL, as shown in the results between Δx_v and the optimized Δx_{r_0}. We have chosen to limit the smallest $\mathcal{N}_{r_0}$ value to 256 in the numerical wave propagation simulator, as seen in Table 2 for a_g equal to 3 or 4. The $a_g = 5$ case allowed for $\mathcal{N}_{r_0}$ to grow beyond 256 and still show correct PLL performance. Thus, the correct number of spatial samples can be ascertained from Eq. (30).

Figure 2 shows the RMS wavefront phase distribution using 10,000 realizations for the numerical wave propagation simulation and the Zernike based approach. The Zernike method uses $J = 528$. The numerical wave propagation method uses Eqs. (28) and (30). One can see that there is excellent agreement between the two simulation approaches in their RMS wavefront distributions. Also note that the distributions have relatively long tails, similar to the real world astronomy results shown in [11]. As expected, the distribution also shows a broadening and a shift to the right as the turbulence strength is increased. Extremely high levels of turbulence lead to very small probabilities of a lucky look, as discussed in [4].

Table 3 shows some of the same validation metrics from [3], but here we use Eqs. (28) and (30) for the sampling parameters. Note that we still see good agreement with these metrics using the proposed sampling criteria. Thus, we have not lost any performance using the proposed sampling and have improved with regard to the PLL statistics. The Fried parameter, isoplanatic angle, θ_0, and RMS Z-tilt still retain relatively small percent errors when compared to their theoretical values. The simulated r_0 value was calculated from the simulators average short exposure PSF, thus providing confirmation the new Δx_{r_0} does not degrade past simulator performance. Additionally, the close match in the RMS Z-tilt between the numerical wave propagation simulator and theoretical value ensures the simulation is producing the correct average long exposure PSF. Average short and long exposure PSF are great metrics to ensure the numerical wave propagation simulator is producing the correct temporal statistics. The correct PLL provides confirmation that the distribution of pupil plane wavefronts, and subsequent turbulent PSFs, matches theory. It is important to note that generating correct temporal statistics [3] does not guarantee the correct PLL as shown in Table 2.

The fact a change in the Nyquist sampling rate does not degrade the existing performance of the simulator is supported by the work in [1] where there is a range of Δx values that could be used in a simulation with a 2-D Gaussian windowed sinc function. However, the work in [19] showed that there is a unique Δx value required to critically sample the simulation and thus produce the correct probability of a lucky look. The work done in [1] still offers significant value for setting other simulation parameters necessary to achieve a valid simulation. Further proof that the numerical wave propagation simulator is not degraded is shown in Sect. 4.C where anisoplantic turbulent frames are shown using the new sampling criteria discussed earlier in this paper.

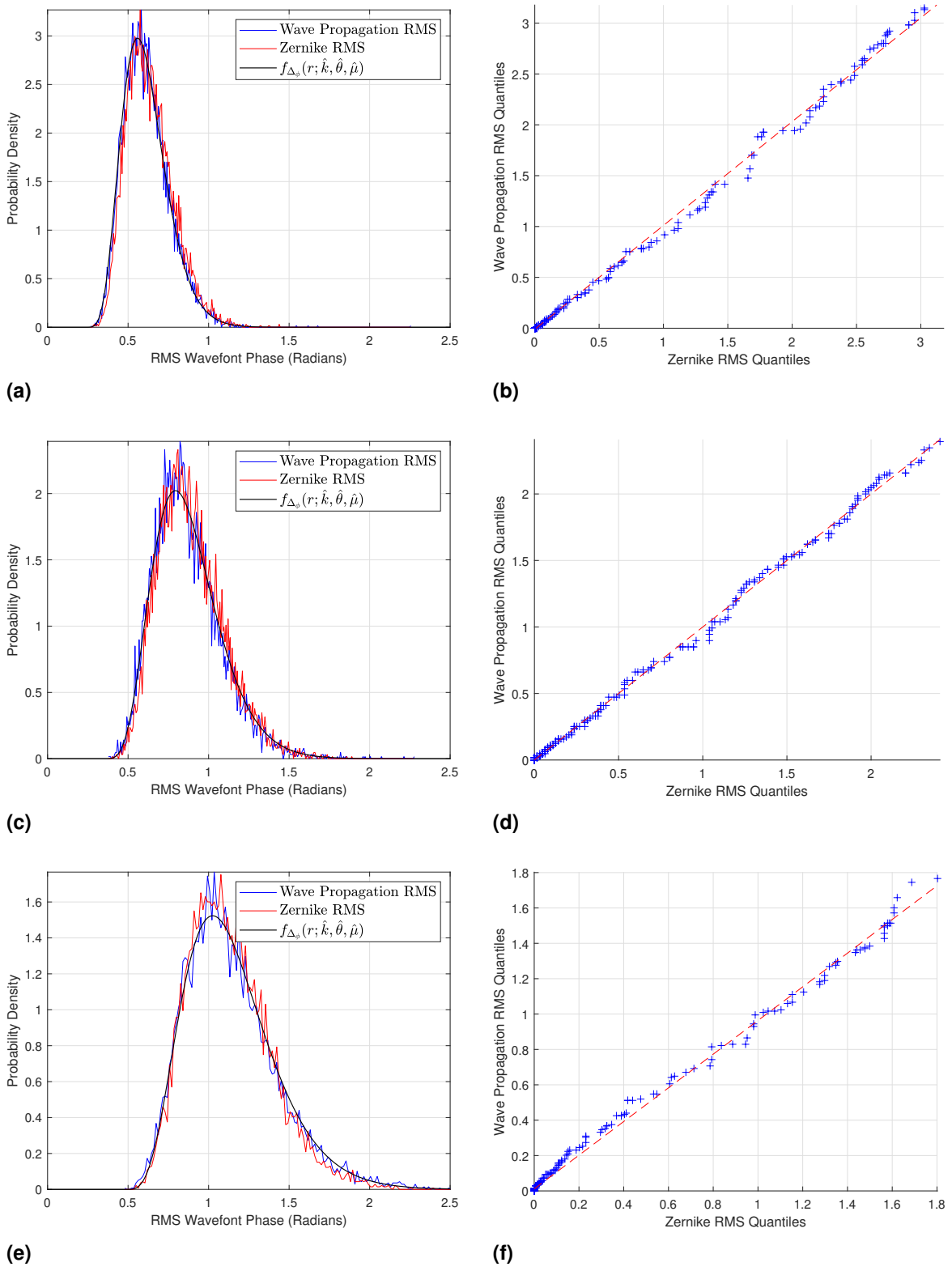

Fig. 2. Histogram plots and quantile-quantile plot between the numerical wave propagation simulator optimized results, with $a_g = 5$, and Zernike based simulator RMS values for (a,b) $D/r_0 = 2$, (c,d) $D/r_0 = 3$, and (e,f) $D/r_0 = 4$.

Table 2. Performance of different spatial samplings over a range of turbulence strengths, varying a_g's, and $c = 1$.

C_n^2 $(m^{-2/3})$	0.284×10^{-15}			0.558×10^{-15}			0.901×10^{-15}		
D/r_0	2			3			4		
Fried PLL [4]	0.986 ± 0.006			0.765 ± 0.005			0.334 ± 0.014		
a_g	3	4	5	3	4	5	3	4	5
Δx_v (mm)	3.789	3.789	3.789	3.789	3.789	3.789	3.789	3.789	3.789
$\mathcal{N}$	256	256	256	256	256	256	256	256	256
PLL	0.992	0.991	0.956	0.815	0.811	0.551	0.434	0.409	0.126
Δx_{r_0} (mm)	5.686	4.325	3.490	5.531	4.235	3.431	5.385	4.148	3.374
$\mathcal{N}_{r_0}$	256	256	328	256	256	352	256	256	364
PLL	0.988	0.987	0.988	0.746	0.763	0.767	0.301	0.333	0.340
Optimal $\Delta\hat{x}$ (mm)	5.668	4.315	3.554	5.507	4.220	3.423	5.354	4.130	3.383
$\mathcal{N}_{r_0}$	256	256	328	256	256	352	256	256	364
Optimal PLL	0.988	0.988	0.986	0.752	0.764	0.765	0.318	0.339	0.334

B. RMS PDF Estimation and Lucky Look OTF

Gladysz, et al., [5] utilized the mean and standard deviation of the RMS phase values to determine the appropriate values of k, θ, and μ. We look to extend the empirical characterization of the three parameter gamma function where the k, θ, and μ parameters are a function of D/r_0 using the numerical wave propagation simulator's RMS distribution for a given D/r_0. The 10,000 independent turbulent wavefront phase realizations were used to help find an optimal equations for k, θ, and μ for a given D/r_0. The MATLAB fminsearch function was used to minimize the Kullback-Leibler divergence metric between the RMS distributions, using the new sampling parameters discussed earlier with $a_g = 5$, and Eq. (7) to determine the optimal equations for twenty equally spaced D/r_0 values from two to four. The optimal equations are

$$\hat{k} = -0.9878(D/r_0) + 9.5029, \tag{31}$$

$$\hat{\theta} = (0.0598(D/r_0) + 0.1080)^2, \tag{32}$$

and

$$\hat{\mu} = (0.1101(D/r_0) + 0.2498)^2. \tag{33}$$

The three parameter gamma PDF with the equations list above were used to plot the probability density curves seen in Fig. 2. Additionally, the new equations can be used with Eqs. (6) and (7) to calculate the PLL for any given $D/r0$ value between two and six. Fried's Eq. (5) is then able to to properly predict the PLL at higher levels of turbulence. The fact the RMS PDF can be used to accurately predict the PLL is plotted in Fig. 3 along with the PLL from the numerical wave propagation simulator using the new sampling criteria. The PLL from the RMS PDF shows excellent agreement with [4] at higher turbulence levels and ties in nicely with Eq. (5), despite the fact k, θ, and μ were determined from the simulator RMS distributions between $2 \leq D/r_0 \leq 4$.

The simulated average lucky look OTF and the β modeled average lucky look OTF using Eqs. (22) and (18) with an RMS threshold of one are shown in Figs. 4(a,c,e) for D/r_0 values equal to two, three, and four, respectively. The average lucky look OTF calculated from the appropriate simulator-generated turbulent PSFs and the modeled average lucky look OTF from Eq. (18) show a high level of agreement. The $D/r_0 = 2$ case shows how the theoretical average lucky look OTF closely matches simulated average short exposure OTF,

Table 3. Comparison between theoretical and statistical parameters from the numerical wave propagation simulator using an $a_g = 5$ and Eq. (28) for Δx_{r_0}.

	$C_n^2 \times 10^{-16}$ ($m^{-2/3}$)		
Parameter	2.838	5.578	9.009
Theoretical r_0 (m)	0.102	0.068	0.051
Simulation r_0 (m)	0.104	0.071	0.053
Percent error	2.134	4.313	4.316
Theoretical θ_0 (μrads)	4.568	3.045	2.284
Simulation θ_0 (μrads)	4.746	3.347	2.560
Percent error	3.904	9.910	12.112
Theoretical RMS Z-tilt (pixels)	1.520	2.132	2.709
Simulation RMS Z-tilt (pixels)	1.524	2.105	2.777
Percent error (%)	0.207	-1.272	2.493

resulting in a very small β as seen in Fig. 5. Note in Fig. 5 that β goes up with increased turbulence level. The reason for this is that lucky selection has a bigger impact at higher turbulence levels. As turbulence levels go up, fewer observed PSFs meet the lucky criterion. This means there is a bigger difference between the average short exposure OTF that accounts for all PSFs, and the lucky look OTF that accounts for only those passing the lucky look test. At lower levels of turbulence, nearly all observed PSFs are considered "lucky" and this means the lucky look OTF is not far from the normal short exposure OTF. However, note that in all cases here β is much lower than the diffraction-limited value of $\beta = 1$. Additionally, the b term was also varied to show how a threshold less than one, $b = 0.8$, generates a less attenuated average lucky look OTF and increases the β value as a function of D/r_0 (see Fig. 5). An optimal β_{opt} value was determined by minimizing the mean absolute error between average lucky look Strehl ratio created from averaging the simulated PSFs that meet the lucky threshold and the modeled average lucky look Strehl ratio calculated from Eq. (18). The optimal β_{opt} varies slightly from the calculated β as shown in Fig. 5 with the RMS thresholds $b = 1$ and $b = 0.8$. The small variation is the difference between β_{opt} and β does not heavily affect the resulting OTFs shown in Fig. 4.

C. Simulation of Anisoplanatic Imagery

Finally, simulated anisoplanatic imagery over a seven kilometer path was generated using the truth frame shown in Fig. 6. The simulated frames with turbulence degradation at three levels is shown in Fig. 7. The numerical wave propagation simulator used the new sampling parameters discussed in Sec. 3, optical parameters presented in Table 1, and simulation parameters in Table 2 [3].

The spatially varying turbulence increases in strength as the D/r_0 value increases, as seen in Fig. 7. We are able to map the corresponding wavefront phase RMS error for each turbulent PSF degrading the frame as well, also shown in Fig. 7. Note that spatially varying wavefront phase RMS values also increase as D/r_0 grows. Lower RMS regions directly correspond to image regions that have not been severely affected by atmospheric turbulence. We believe the intricate structure of the anisoplanatic RMS statistics depited in Fig. 7 capture realistic spatial correlations in the PLL related statistics. The temporal evolution of the spatially varying turbulence and RMS values can be seen in Fig. 8 where a small region of interest was selected for between two sequential turbulent frames using the windspeed in [3]. The spatially varying warp and blur allows for certain regions to increase in resolution and allow for a lucky look through the simulated atmosphere while others decrease and heavily blur the truth scene. To the best of our knowledge, the simulated anisoplanatic spatial structure of wavefront RMS values revealed in Figs. 7 and 8 has not been previously shown in the literature.

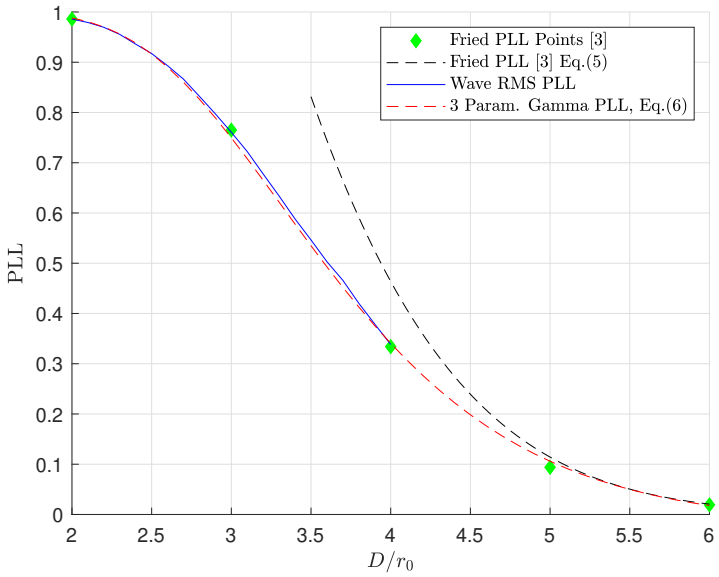

Fig. 3. Various PLL data points and curves showing great agreement between the PLL calculated from the three parameter gamma RMS PDF and numerical wave propagation simulator output using the new sampling criteria.

5. CONCLUSION

In this paper we have shown how to modify the spatial sampling parameter from a vacuum propagation to include turbulence via [20]. The addition of the Fried parameter ensures that the spatial sampling will decrease as the amount of optical turbulence increases along the path. Additionally, the new spatial sampling parameter is informed by the cutoff frequency for a 2-D Gaussian windowed sinc point source. Properly sampling the point source, phase screens, and pupil plane allows for each turbulent wavefront, and subsequent turbulent PSF, to have the correct RMS and contribute to an accurate PLL. This now guarantees the individual turbulent PSFs have the correct spatial structure, along with the correct temporal structure to match the average short and long exposures. Thus, the optimized Δx_{r_0} values do not degrade performance of the existing numerical wave propagation simulator.

Wavefront phase RMS distributions for the numerical wave propagation simulator and Zernike based simulation show excellent agreement. Zernike wavefront phase simulators are extremely powerful and fast for isoplanatic applications when generating independent PSFs. Research has been conducted on generating the temporal evolution of a turbulent PSF over an isoplanatic patch [23], and how to achieve spatial evolution across portions of a frame [24]. The numerical wave propagation simulator incorporates large phase screens that produce the accurate temporal and spatial PSF correlations over the sensor field of view. However, the numerical wave propagation has a relatively high computational cost. All of these simulation methods have relative merits and can be valuable tools in understanding turbulence and evaluating turbulence mitigation methods.

Updated equations of the three parameter gamma model based upon the D/r_0 turbulence strength were discussed and the goodness of fit between the three parameter gamma RMS PDF and simulated RMS distributions was presented. The new three parameter gamma RMS PDF also aided in calculating the correct PLL for a wide range of D/r_0 values and bridged the gap between weak turbulence and the PLL equation defined in [4]. Additionally, a novel average lucky look OTF was defined by fusing the diffraction OTF and average short exposure OTF. The average lucky look OTF calculation utilized the new RMS PDF and can be calculated for a given D/r_0 in weak turbulence, RMS threshold, and level of registration accuracy. RMS mapping of turbulent imagery was also added to the simulator to provide insight into the amount of spatially varying blur seen in newly simulated anisoplanatic turbulence imagery.

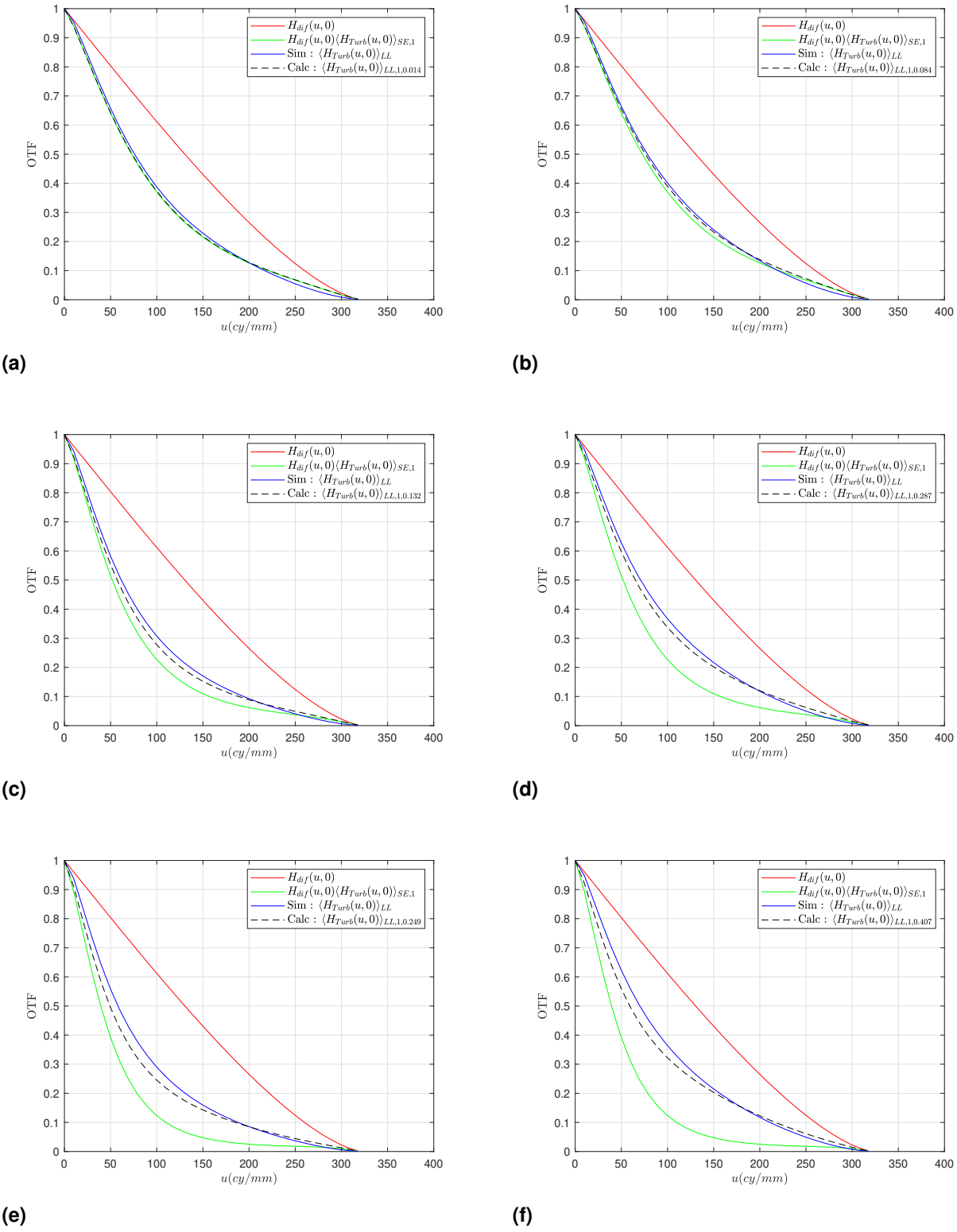

Fig. 4. Average lucky look OTFs calculated from the numerical wave propagation simulator outputs using the new sampling criteria and the corresponding calculated average lucky look OTF model incorporating the new β value calculated from Eq. (22). Sub figures (a), (c), (e) utilize an RMS threshold of one, i.e. $b = 1$, while (b), (d), (f) use $b = 0.8$ where (a,b) $D/r_0 = 2$, (c,d) $D/r_0 = 3$ and (e,f) $D/r_0 = 4$.

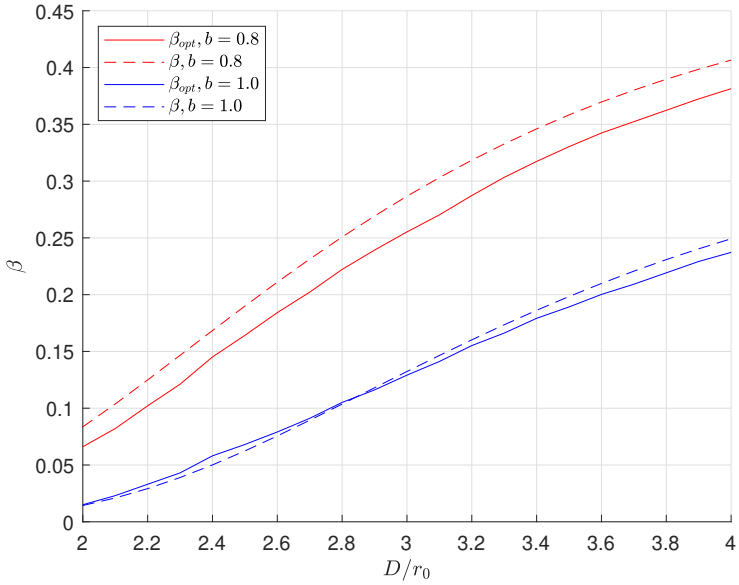

Fig. 5. The optimized β_{opt} value versus the calculated β value from Eq. (22) for different b RMS thresholds.

Fig. 6. The ideal truth frame.

Funding. This work has been supported in part under AFRL Award No. FA8650-17-D-1801 and has been cleared for public release with the case number AFRL-2021-1082.

Acknowledgments. The authors would like to thank Kenneth Barnard, Phil Plummer, and Todd Rovito at AFRL for providing support for this project. We would also like to thank Darwin Adams, Michelle McDaniel, and others at the High Performance Computing Modernization Program for their assistance in getting the numerical wave propagation simulator code up and running to generate the large data sets used for this project.

Disclosures. The authors declare no conflicts of interest.

Data availability. Data underlying the results presented in this paper are available the miscellaneous folder, filename 5.2.10 titled stream and bridge, Ref. [25].

REFERENCES

1. J. D. Schmidt, *Numerical Simulation of Optical Wave Propagation with Examples in MATLAB*, SPIE Press Monograph (SPIE Press, 2010).
2. J. P. Bos and M. C. Roggemann, "Technique for simulating anisoplanatic image formation over long horizontal paths," Opt. Eng. **51** (2012).
3. R. C. Hardie, J. D. Power, D. A. LeMaster, D. R. Droege, S. Gladysz, and S. Bose-Pillai, "Simulation of anisoplanatic imaging through optical turbulence using numerical wave propagation with new validation analysis," Opt. Eng. **56**, 071502 (2017).
4. D. L. Fried, "Probability of getting a lucky short-exposure image through turbulence," JOSA **68**, 1651–1658 (1978).
5. S. Gladysz, J. C. Christou, L. W. Bradford, and L. C. Roberts, "Temporal variability and statistics of the strehl ratio in adaptive-optics images," Publ. Astron. Soc. Pac. **120**, 1132 (2008).

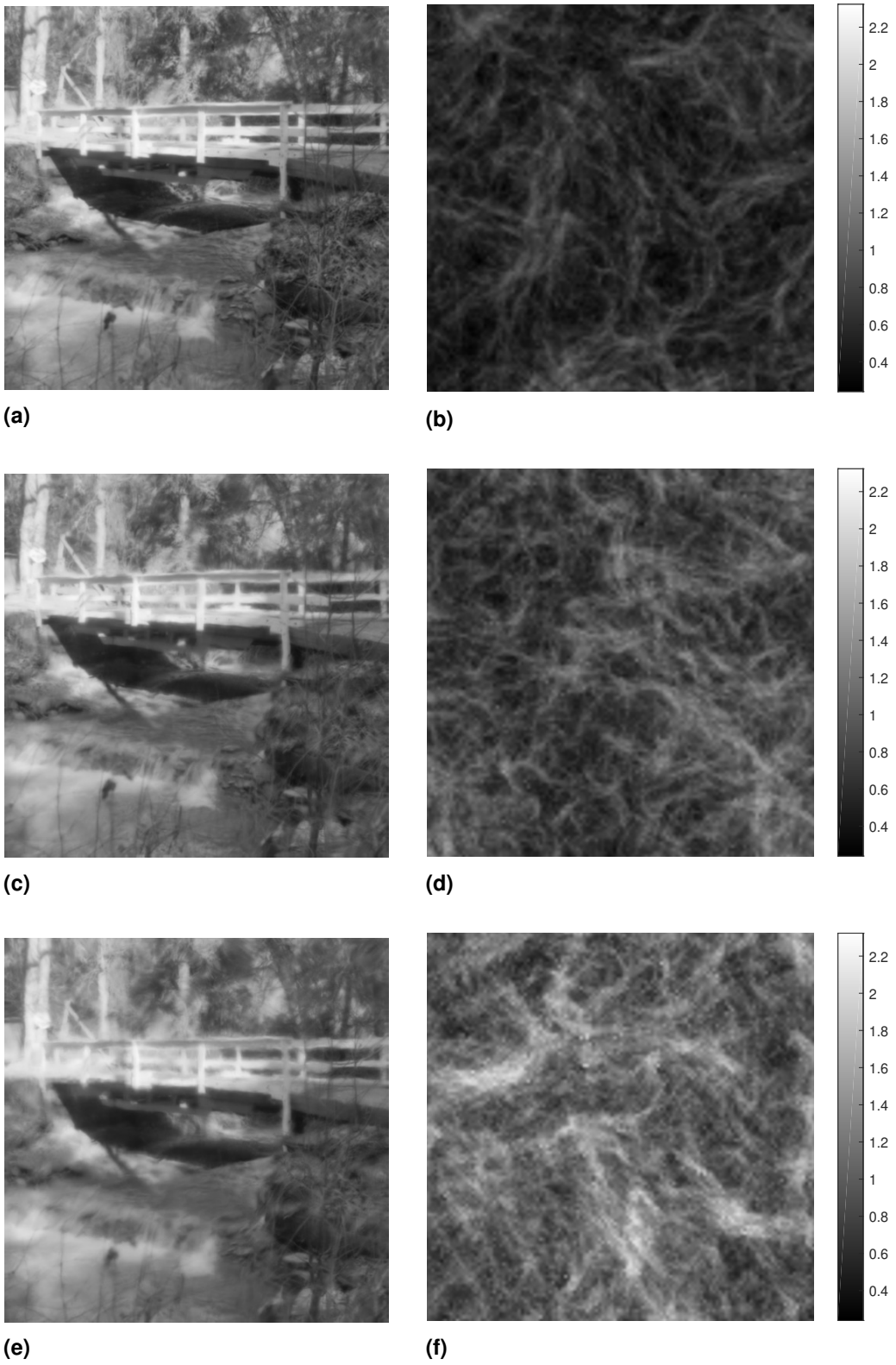

Fig. 7. The simulated anisoplanatic turbulent image using the new sampling criteria for (a) $D/r_0 = 2$, (c) $D/r_0 = 3$, and (e) $D/r_0 = 4$. Wavefront phase RMS spatial mapping of the turbulent imagery is shown in (b) $D/r_0 = 2$, (d) $D/r_0 = 3$, and (f) $D/r_0 = 4$.

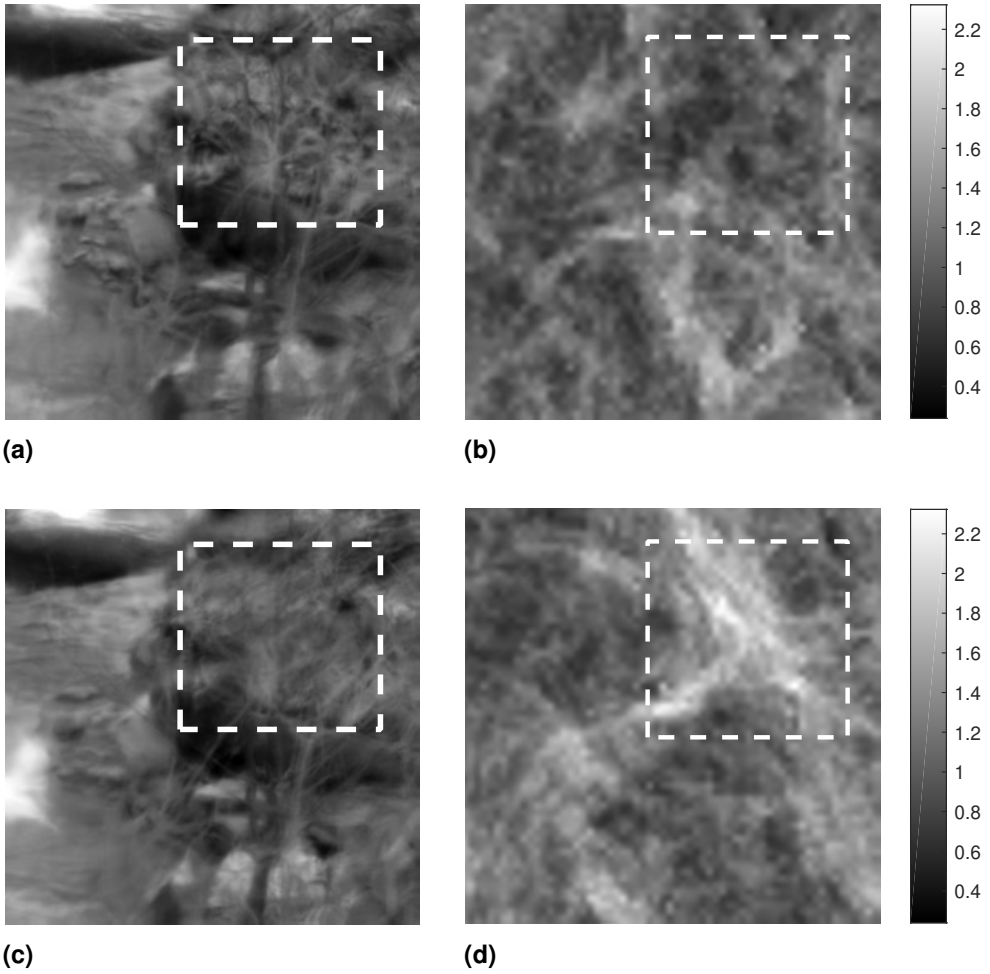

Fig. 8. Two anisoplanatic turbulent regions of interest with $D/r_0 = 4$ where (a,c) are the turbulent images and (b,d) are the wavefront phase RMS spatial mapping of the corresponding turbulent images. Dashed line rectangles show how strong wavefront phase RMS leads to more blurring while weaker wavefront phase RMS leads to less blur.

6. J. W. Goodman, *Introduction to Fourier optics* (Roberts and Company Publishers, 2005).
7. D. L. Fried, "Optical resolution through a randomly inhomogeneous medium for very long and very short exposures," JOSA **56**, 1372–1379 (1966).
8. N. A. Roddier, "Atmospheric wavefront simulation using zernike polynomials," Opt. Eng. **29**, 1174–1181 (1990).
9. R. J. Noll, "Zernike polynomials and atmospheric turbulence," JOSA **66**, 207–211 (1976).
10. G.-M. Dai, "Wavefront simulation for atmospheric turbulence," in *Image Reconstruction and Restoration,* vol. 2302 (International Society for Optics and Photonics, 1994).
11. J. Baldwin, P. Warner, and C. Mackay, "The point spread function in lucky imaging and variations in seeing on short timescales," Astron. & Astrophys. **480**, 589–597 (2008).
12. L. C. Roberts Jr, M. D. Perrin, F. Marchis, A. Sivaramakrishnan, R. B. Makidon, J. C. Christou, B. A. Macintosh, L. A. Poyneer, M. A. van Dam, and M. Troy, "Is that really your strehl ratio?" in *Advancements in Adaptive Optics,* vol. 5490 (International Society for Optics and Photonics, 2004), pp. 504–515.
13. B. R. Hunt, A. L. Iler, C. A. Bailey, and M. A. Rucci, "Synthesis of atmospheric turbulence point spread functions by sparse and redundant representations," Opt. Eng. **57**, 024101 (2018).
14. J. W. Goodman, *Statistical optics* (John Wiley & Sons, 2015).
15. M. Born and E. Wolf, "Basic properties of the electromagnetic field," Princ. optics **44** (1980).
16. H. Stark and J. Woods, *Probability and Random Processes with Applications to Signal Processing* (Prentice-Hall, Inc., 2002).
17. R. C. Hardie, M. A. Rucci, A. J. Dapore, and B. K. Karch, "Block matching and wiener filtering approach to optical turbulence mitigation and its application to simulated and real imagery with quantitative error analysis," Opt. Eng. **56**, 071503 (2017).
18. M. T. Eismann and D. A. LeMaster, "Aerosol modulation transfer function model for passive long-range imaging over a nonuniform atmospheric path," Opt. Eng. **52**, 1 – 14 (2013).
19. D. G. Voelz, *Computational fourier optics: a MATLAB tutorial* (SPIE Press, 2011).
20. J. D. Mansell, R. Praus, and S. Coy, "Determining wave-optics mesh parameters for complex optical systems," in *Optical Modeling and Performance*

Predictions III, vol. 6675 (International Society for Optics and Photonics, 2007), p. 66750H.
21. D. L. Knepp, "Multiple phase-screen calculation of the temporal behavior of stochastic waves," Proc. IEEE **71**, 722–737 (1983).
22. M. A. Herráez, D. R. Burton, M. J. Lalor, and M. A. Gdeisat, "Fast two-dimensional phase-unwrapping algorithm based on sorting by reliability following a noncontinuous path," Appl. optics **41**, 7437–7444 (2002).
23. I. B. Putnam and S. C. Cain, "Modeling a temporally evolving atmosphere with zernike polynomials," in *Advanced Maui Optical and Space Surveillance Technologies (AMOS) Conference,* (2012).
24. N. Chimitt and S. H. Chan, "Simulating anisoplanatic turbulence by sampling intermodal and spatially correlated Zernike coefficients," Opt. Eng. **59**, 1 – 26 (2020).
25. http://sipi.usc.edu/database/.